energies

MDPI

Article

The Effective Field in the T(x) Hysteresis Model

Krzysztof Roman Chwastek [1,*], Paweł Jabłoński [1], Dariusz Kusiak [1], Tomasz Szczegielniak [1], Václav Kotlan [2] and Pavel Karban [2]

[1] Faculty of Electrical Engineering, Częstochowa University of Technology, 42-201 Częstochowa, Poland
[2] Faculty of Electrical Engineering, University of West Bohemia, 304 14 Pilsen, Czech Republic
* Correspondence: krzysztof.chwastek@pcz.pl

Abstract: Hysteresis loops constitute the source of important information for the designers of magnetic circuits in power transformers. The paper focused on the possibility to interpret the phenomenological T(x) model in terms of effective field vs. magnetization dependence. The interdependence of anhysteretic curve and hysteresis loops was emphasized. The concept of the anhysteretic plane introduced at the end of the last century by Sablik and Langman was subject to a tangible interpretation within the hyperbolic model framework. A novel geometric interpretation of the "effective field" related to the concept of affine transformation was introduced. It was shown in the paper that minor hysteresis loops of grain-oriented electrical steel may be described with the proposed formalism.

Keywords: modeling; T(x) model; geometric interpretation; electrical steel

check for updates

Citation: Chwastek, K.R.; Jabłoński, P.; Kusiak, D.; Szczegielniak, T.; Kotlan, V.; Karban, P. The Effective Field in the T(x) Hysteresis Model. *Energies* **2023**, *16*, 2237. https://doi.org/10.3390/en16052237

Academic Editors: Tomasz Popławski, Marek Kurkowski and Enrique Romero-Cadaval

Received: 3 February 2023
Revised: 21 February 2023
Accepted: 24 February 2023
Published: 25 February 2023

1. Introduction

Power and distribution transformers are electric devices that play a crucial role in power engineering. The IEEE Standard C57.12.80-2010 defines a power transformer as a transformer which transfers electric energy in any part of the circuit between the generator and the distribution primary circuits, whereas a distribution transformer is used for transferring electrical energy from a primary distribution circuit to a secondary distribution circuit or consumer's service circuit [1]. One of important issues in transformer design is the optimization of their magnetic circuits, both in terms of geometric structure and the grade of soft magnetic material used [2,3].

The magnetic circuits of these devices are assembled of grain-oriented (GO) electrical steel. Grain-oriented steel features a strong preferred crystallographic orientation (magnetic anisotropy). In iron crystals the so-called easy magnetization directions are along their edges, i.e., along the $\langle 001 \rangle$ directions. The ground-breaking achievement in GO metallurgy leading to significant improvement of their magnetic properties was the 1935 technology developed by Goss, who suggested that preferable orientation for the iron crystals should be such that the crystal planes $\{110\}$ are oriented parallel to the steel surface, whereas the directions $\langle 001 \rangle$ are parallel to the rolling direction. More information on the relevance of the Goss texture for electrical steels in case of transformer applications and other metallurgy-related issues may be found, e.g., in ref. [4].

Grain oriented steel is composed of large grains exhibiting the Goss texture, as depicted in Figure 1. It is remarkable that in the GO steel grains are considerably large and visible with naked eyes (from a few millimeters to a few centimeters). As a consequence, GO electrical steel has excellent magnetic properties (coercive field strength in the range 4–20 A/m and maximum permeability values around 7×10^4—these values differ by about an order of magnitude from those typically found in non-oriented steels) [5].

Understanding metallurgical processes during GO electrical steel production and phenomena occurring during its re-magnetization is crucial for the optimization of the working conditions of magnetic circuits. Thanks to the advances in steel manufacturing technologies during the last century, a significant improvement of magnetic properties for

GO steel has been achieved, cf. Figure 2, which depicts the reduction of specific power loss density due to improvements in processing technology over the years.

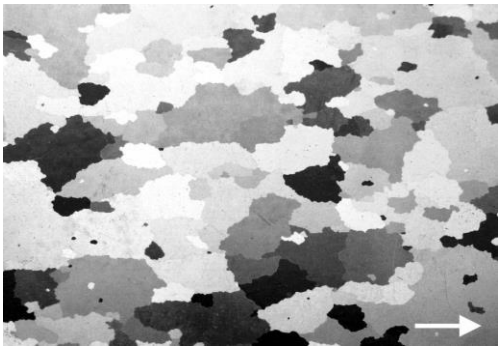

Figure 1. A photograph of the polycrystalline structure of GO steel after removal of isolating coatings. The arrow size on the photo is around 1 cm, whereas its direction depicts the rolling direction. Source: Encyclopedia Magnetica, https://e-magnetica.pl/file/grains_in_go_steel_jpg, author: Stan Zurek, license: CC-BY-4.0 (accessed on 1 November 2022).

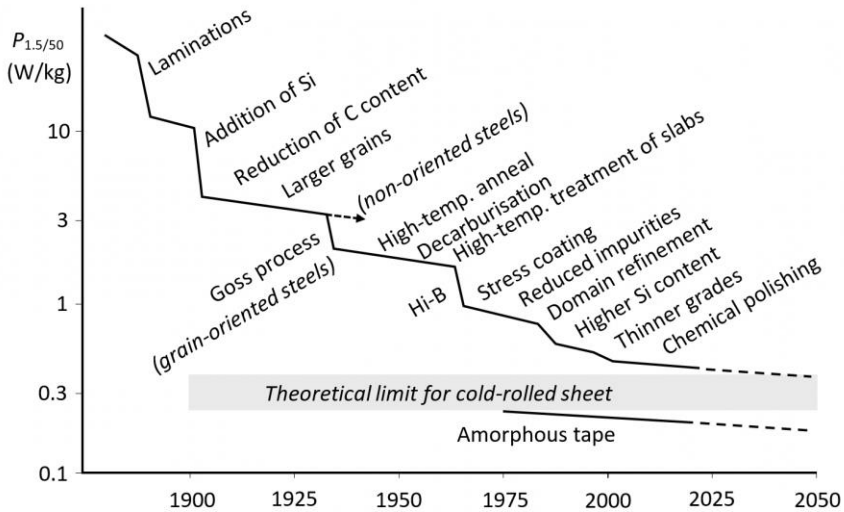

Figure 2. Reduction of specific power density due to improvements in GO processing technology. Source: Encyclopedia Magnetica, https://e-magnetica.pl/file/electrical_steel_progress_magnetica_png. author: Stan Zurek, license: CC-BY-4.0 (accessed on 1 November 2022).

Contemporary grain-oriented steels may be classified as conventional grain-oriented (CGO) and high grain-oriented (HGO) steels. In conventional grades, the average dispersion of grain directions from the rolling direction is of the order of 7 degrees, which makes it possible to obtain magnetic induction B10 at the 1.85 T level (B10 is the abbreviation for a figure of merit used by steel producers; it denotes magnetic induction measured at H = 1 kA/m). In HGO steels the texture is more perfect, i.e., the average dispersion of grain directions does not exceed 4 degrees, which in turn implies a higher value of B10, which may achieve 1.95 T; moreover, these grades feature significantly lower loss densities (around 20%) in comparison with CGO steels.

In order to minimize the core losses of ready-made GO steels, a number of additional treatment processes aimed at domain refinement have been proposed. Mechanical scratching, plasma irradiation, spark ablation, and laser scribing have been used for many years. All these methods can provide favorable stress conditions and thereby refine the magnetic domains because of mechanical- or thermal-induced strains [6]. Among the aforementioned techniques, laser scribing has gained a lot of attention due to its process flexibility and non-contact nature.

Another tendency in contemporary GO steel manufacturing is an attempt to produce ultra-thin grades (with thicknesses equal to 0.1 mm or less) [7]. Until recently, such thin sheets were produced by JFE Steel, a manufacturer of high-silicon (6.5% wt. Si) non-oriented steel [8,9].

Despite enormous efforts made over the years in processing technology (cf. Figure 2), it is estimated that energy losses in magnetic circuits of transformers still account for 5–10% of the total electric energy produced worldwide [10]. In the European Union the losses for distribution transformers are estimated at 33 TW · h/year [11,12]. It should be remembered that most transformers work continuously for at least 25–30 years.

Figure 3 depicts an exemplary power transformer.

Figure 3. A photo of a high-voltage (750 kV) power transformer. Source: Wikimedia Commons repository, author: Novoklimov, https://commons.wikimedia.org/wiki/ File: High-voltage_transformer_750_kV_Трансформатор_750_кВ.jpg (accessed on 1 November 2022).

In order to assess the level of development for a given country, one can take into account the amount of consumed electric energy. This quantity is quite well correlated with the volume of produced GO electrical steel since this material cannot be easily replaced with any other soft magnetic material to serve as the core material in magnetic circuits of power and distribution transformers [13]. The main factor stimulating the growing energy demand worldwide is industrial growth, e.g., in China or India. Moreover, the existing infrastructure has to be constantly replaced in order to increase the electrical power generating capacity. According to the estimates of the International Energy Agency, it is predicted that until 2030 this quantity is to rise at 3% rate per annum all over the world (about 150 GW) [14].

In order to optimize the design of magnetic circuits in transformers, it is necessary to work out appropriate descriptions of magnetic properties of GO electrical steel. The present paper focused on modeling minor hysteresis loops using the T(x) approach combined with the concept of effective field. This description is valuable because of the relatively simple mathematical apparatus and strictly defined rules for predicting the system response at an arbitrary excitation signal.

The paper is structured as follows: Section 2 covers basic information on the concept of effective field and on the Jiles–Atherton hysteresis model, which is probably the most wide-spread description on the "effective field". Another important concept, also rooted in the JA formalism, is the anhysteretic curve. In the successive part of the section, the T(x)

model is briefly outlined. It is shown that the anhysteretic curve may be easily recovered from the relationships for the upward and downward loop branches, thus contrary to the JA model, in which the equation for the anhysteretic curve is set arbitrarily; the T(x) approach offers a more comprehensive picture of the hysteresis phenomenon. It is shown that the anhysteretic curve may possess inflection points for higher values of reduced coercive field strength; previously, this fact was interpreted by some authors in terms of the possible presence of multiple phases within the material, though in the present paper it is shown that this effect is merely a consequence of strictly prescribed mathematical formalism. A practical algorithm for the determination of anhysteretic curves is outlined. Moreover, in this section it is shown that there exist local anhysteretic curves corresponding to their hysteresis counterparts (symmetric minor loops). This observation allows us to explain the concept coined twenty-seven years ago by Sablik and Langman, who envisaged the "anhysteretic plane" when interpreting measurement results for samples subjected to different excitation conditions.

Section 3 is devoted to a comparison of experimental data with modeling results. At first, an interpretation of the T(x) model in physical units, proposed some time ago by the first author of the present contribution, is recalled. The most interesting part of the section is—in our opinion—devoted to two approaches allowing one to transform minor hysteresis loops in dimensionless units into physically tangible curves. The second approach is inspired by the geometric interpretation of the "effective field", related to the concept of affine transformation. Recalling the transformation matrix for rotation, a similar transformation matrix, in which magnetization remains is invariant, is proposed. It is shown that this approach leads to modeled hysteresis curves with lower dynamic susceptibilities than those generated by the approach based on straightforward substitution of respective relationships into model equations. Finally, in this section we provide a modeling example for an increased excitation frequency (chosen as mains frequency because of the practical application). In order to extend the T(x) model with effective field into dynamic conditions, we "dress up" quasi-static loops with an extra non-linear term; thus, our approach is basically derived from a two-term separation formula. The dynamics are controlled by the exponent appearing in the power law, which may be derived from experimental dependence $H_c(f) - H_{c0}$.

Section 4 includes some extra information on alternative hysteresis models applied to similar problems and outlines possible topics for future work. Finally, Section 5 section summarizes the paper's contents and the obtained results.

2. Theoretical Foundations

2.1. The Effective Field

The concept of effective field plays an important role in contemporary physics and engineering. The effective field is a useful framework which allows one to take into account the equivalent response from several physical phenomena, including the internal coupling mechanism, induced and residual mechanical stresses, and thermal and magnetic viscosity [15] acting on the considered fragment of matter (in ferromagnetism on a specimen; specifically, in the context of this paper, on a sheet of GO steel). Thus, the concept lies at the core of the operating principle of different physical sensors.

Among the many descriptions of ferromagnetic hysteresis, the formalism developed in the in the 1980's by Jiles and Atherton [16] gained quite a lot of attention from the scientific community due to the relatively uncomplicated structure of its equations, allowing one for simple numerical implementation. The "effective" field, being the true field within magnetic material, appeared as the argument in the fundamental ordinary differential equation of the JA description; thus, it constituted the "backbone" of the formalism. The evolution of the Jiles–Atherton (JA) model equations and their different forms are reviewed, e.g., in [17,18].

An important paper focused on the (lack of) physical foundations underlying the original JA description was the paper by Zirka et al. [19]. This publication focused on the

modified Langevin function used for the description of anhysteretic magnetization. The argument of the anhysteretic function was the "effective" field; thus, in the JA model there existed an implicit coupling between the irreversible and the reversible magnetization components. The decomposition of total magnetization into these two components was argued, pointing out that a description correct from the point of irreversible thermodynamics should rather rely on the decomposition of total field strength (as is carried out in the Harrison model [20]).

Since the physical foundations of the Jiles–Atherton formalism have been put into question, in particular the possibility to use the modified Langevin function for the description of the anhysteretic magnetization, in the present paper we focused on another model of hysteresis curves, namely, the T(x) model [21].

2.2. The Anhysteretic Curve

There is a general agreement between scientists that the anhysteretic curve should be related to the description of magnetization process in an ideal material devoid of structural defects or other hindrances to the domain wall movement, referred to as pinning sites [22–24]. In reality, such materials do not exist; thus, it might seem that the concept of the anhysteretic curve is vague and unclear. What is even worse, there is an on-going debate between researchers regarding how to reproduce the anhysteretic curve experimentally, cf., [25,26].

However, the concept of the anhysteretic curve obtains a clear and tangible physical interpretation if one considers it from a thermodynamical perspective. This curve corresponds to the global equilibrium state of the ferromagnetic material [25].

2.3. The T(x) Hysteresis Model

The T(x) model is a phenomenological description, based on extensive use of hyperbolic tangent transformation. The anhysteretic curve was obtained in this model by averaging the output variable y values read from the ascending and the descending loop branches.

Symmetric loop branches are described in T(x) model as

$$y(x) = \tanh(x \mp a_0) \pm b \tag{1}$$

where the meaning of a_0 is coercive field strength expressed in dimensionless units, whereas b is introduced in order to match loop ends for lower excitation levels (for minor loops)

$$b = 0.5[\tanh(x_\mathrm{m} + a_0) - \tanh(x_\mathrm{m} - a_0)] \tag{2}$$

where x_m is the value of the input variable for which both loop branches coincide. The description is easily adjustable for asymmetric excitation conditions, cf., [21,27]. In order to simplify the notation, we write $T(x)$ for $\tanh(x)$.

Within the T(x) model framework the anhysteretic curve encompasses the loci of minor loop tips; thus, the following relationship may be written

$$y_\mathrm{anh}(x) = 0.5[T(x + a_0) + T(x - a_0)] \tag{3}$$

Figure 4 depicts the shapes of simulated hysteresis and anhysteretic curves for two arbitrarily chosen values of a_0. The following can be easily noticed:

- The anhysteretic curves are monotonous; they pass through the first and the third quadrant of the $(x, y(x))$ plane and possess a saturation feature;
- For a sufficiently large value of coercive field strength, the shape of the anhysteretic curve given in (3) exhibits inflection; thus, it is similar to the shape of magnetization curves recorded for two-phase magnetic materials [28]. Since the T(x) model is a purely phenomenological tool, the presence of inflection points on the simulated anhysteretic curve cannot be attributed to the onset of a new physical phenomenon or the disclosure of some extra phase in the material; rather, it is a natural consequence

of mathematical formalism and the assumption that all symmetric loop tips belong to the anhysteretic curve.

At this point it should be pointed out that the T(x) approach may be extended to multi-phase compounds in a simple way; this is achieved by summing the (weighted) contributions from individual alloy phases, as demonstrated in [29,30]. The concept was successfully verified in a study of temperature-dependent hysteresis curves for a magnetocaloric composite based on La(Fe, Mn, Si)13-H type alloys [31].

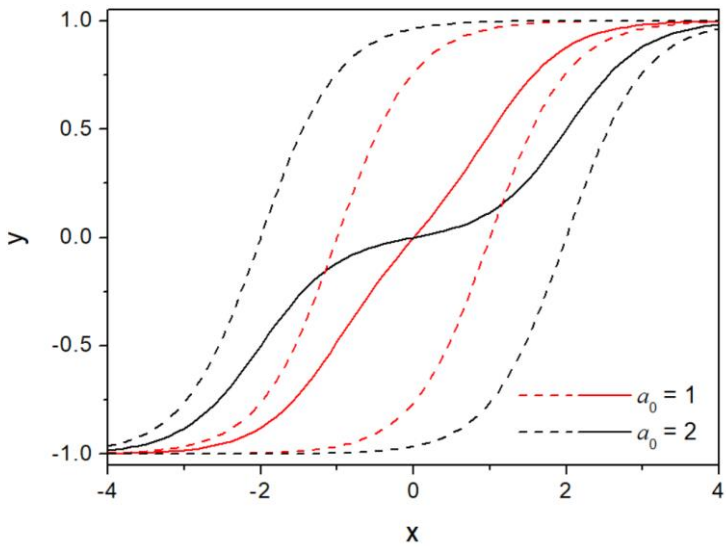

Figure 4. Simulated major hysteresis loops (dashed line) and anhysteretic curves (solid lines) for two values of the reduced coercive field (a_0 = 1, 2 using Takács' notation) and $x_m = 4$.

An in-depth inspection of relationships (1)–(3) allows one to draw a conclusion that both descriptions, i.e., of the hysteresis loop branches and of the anhysteretic curve are mutually inter-related. This fact was stressed in [32]. For the specific choice of hyperbolic tangent as the design curve, one can use the identity of $T(x \pm a_0) = [T(x) \pm T(a_0)]/[1 \pm T(x)T(a_0)]$.

Since $y_{\text{anh}} = 0.5[\ T(x - a_0) + T(x + a_0)]$ then

$$2y_{\text{anh}} = \frac{T(x) - T(a_0)}{1 - T(x)T(a_0)} + \frac{T(x) + T(a_0)}{1 + T(x)T(a_0)} = \frac{T(x) - T(a_0) + T^2(x)T(a_0) - T(x)T^2(a_0) + T(x) + T(a_0) - T^2(x)T(a_0) - T(x)T^2(a_0)}{1 - (T(x)T(a_0))^2} \quad (4)$$

which reduces to the following expression:

$$2y_{\text{anh}} = \frac{2T(x)\left(1 - T^2(a_0)\right)}{1 - (T(x)T(a_0))^2} \quad (5)$$

A conclusion may be drawn that the recovery of the anhysteretic curve from loop branches as their middle curve, suggested, e.g., by Krah and Bergqvist [33], is justified. This fact has far-reaching consequences since it allows one to avoid tedious point-by-point measurements, cf., Figure 5.

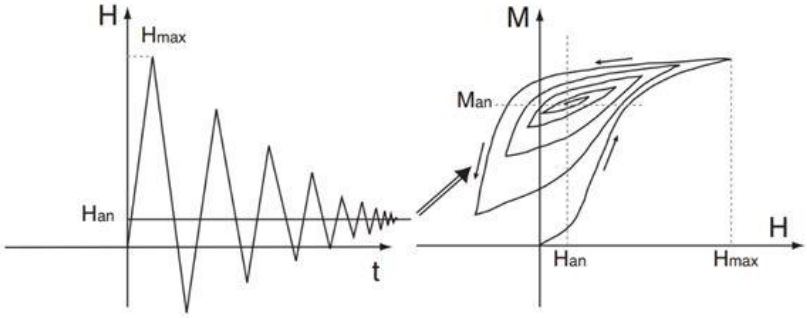

Figure 5. The "classical" method to recover a single point on the anhysteretic curve by the application of decaying alternating field at a given bias level; this procedure has to be repeated many times, and it is thus tedious and time-consuming.

The relationship (7) may be transformed to isolate $T(x)$ as a function of y_{anh}; thus, the inverse anhysteretic function may be recovered:

$$\left(1 - T^2(a_0)T^2(x)\right)y_{\text{anh}} = T(x)\left(1 - T^2(a_0)\right) \tag{6}$$

$$T^2(x)y_{\text{anh}}T^2(a_0) + T(x)\left(1 - T^2(a_0)\right) - y_{\text{anh}} = 0 \tag{7}$$

If $y_{\text{anh}} = 0$ then the degenerated solution is $T(x) = 0$, $x = 0$, otherwise $T(x)$ is computed as the positive root of the quadratic equation $AT^2(x) + BT(x) + C = 0$,

$$T(x) = \frac{-B + \sqrt{\Delta}}{2A} = \frac{-\left(1 - T^2(a_0)\right) + \sqrt{\left(1 - T^2(a_0)\right)^2 + 4y_{\text{anh}}^2 T^2(a_0)}}{2y_{\text{anh}}T^2(a_0)} \tag{8}$$

and finally, x is computed from the atanh function (inverse hyperbolic function). This expression is provided in Takács' textbook [21] (page 22).

The importance of the relationship (10) is in the fact that it is valid regardless of the interpretation of x. Thus, x may be interpreted as the reduced effective field [34].

The computation flowchart may be summarized as follows:

1. Set the value for a_0;
2. Set the limiting value for y_{m}, $-1 < y_{\text{m}} < 1.$;
3. Compute $T(x_{\text{m}})$ from (10);
4. Compute x_{m} using the hyperbolic area tangent function;
5. Compute b from (4);
6. For successive values of $y \in \langle -y_{\text{m}};\ y_{\text{m}} \rangle$, compute the corresponding x values for the ascending and the descending loop branches from transformed (3), solved for x. If necessary, compute the values of anhysteretic field strength via (10).

It can be easily noticed that this computation chain is typical for an inverse model, in which the magnetic field strength is a function of magnetization.

Figure 6 depicts a family of simulated minor hysteresis loops (solid lines) and anhysteretic curves (dashed lines) for the fixed value $a_0 = 2$ and for different amplitudes y_{m} = 0.95, 0.75, 0.5, and 0.25. The interpolated value of coercive field strength for y_{m} = 0.95 is 1.95; thus, this loop approaching saturation can be considered as the major loop. It can be noticed that the slopes of anhysteretic curves depend on the excitation amplitude: as y_{m} decreases, the slope $\mathrm{d}x_{\text{anh}}/\mathrm{d}y$ (i.e., the reciprocal of reduced anhysteretic susceptibility) increases for the same y.

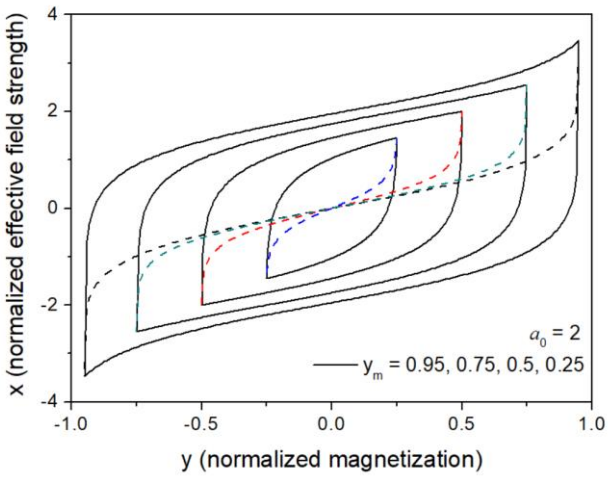

Figure 6. A family of simulated symmetric hysteresis loops and the corresponding anhysteretic curves for $a_0 = 2$.

A detailed inspection of Figure 6 leads to the conclusion that there is no single universal anhysteretic curve valid in the whole $H = H(M)$ plane, since for each amplitude of the loop, one can distinguish a local anhysteretic curve corresponding to the minor loop. This fact has been mentioned in several papers, including the "offset anhysteretics" in the conclusions of the paper [35] (the authors could not provide an interpretation of this effect). An important contribution towards developing a better understanding of the anhysteretic concept is represented by the paper by Sablik and Langman, who envisaged the whole family of anhysteretic curves obtained for different excitation conditions as a plane [36]. The present paper extended their reasoning to describe the case of symmetric minor loops for a GO steel sample.

3. Modeling

3.1. Modeling in Quasi-Static Excitation Conditions

The original T(x) model was defined in terms of dimensionless quantities x and y. Their physical interpretation was proposed in ref. [34], in which x was interpreted as a reduced "effective field", by analogy to the JA model, whereas y as reduced magnetization.

The T(x) model may be written in physical units for symmetric excitation as

$$M = M_s \tanh \frac{H_{eff} \mp H_c}{a} \pm b\left(H_{eff}^{TIP}, M^{TIP}\right) \tag{9}$$

in which H_{eff} is defined as $H_{eff} = H + \alpha M$, whereas

$$b\left(H_{eff}^{TIP}, M^{TIP}\right) = 0.5 M_s \left[\tanh \frac{{H_{eff}}^{TIP} + H_c}{a} - \tanh \frac{{H_{eff}}^{TIP} - H_c}{a}\right] \tag{10}$$

It can be noticed that the T(x) model requires the knowledge of coercive field strength H_c for the major loop. The model parameters are saturation magnetization M_s, A/m, coercive field strength H_c, A/m, the dimensionless Weiss' coefficient α, accounting for mutual interactions between magnetic moments within the material (it appears in the second term of the assumed definition for the effective field $H_{eff} = H + \alpha M$), and the parameter a, A/m, which basically controls the loop shape. The values of model parameters have to be determined on the basis of magnetic measurements.

The nominal thickness of grain-oriented steel used in magnetic circuits of power transformers is in the range 0.27–0.35 mm (here we did not take into account the ultra-thin gauges, mentioned in ref. [7] and the Introduction section). For model verification we chose a sheet of ET 122-30 grade (0.3 mm thick). Hysteresis loops were measured using a single-sheet tester device and a computer-aided measurement setup, whose fundamental

parameters were provided in a recent publication [37]. The excitation frequency was 5 Hz, which can be considered as approaching a quasi-static (DC) condition, since this value lies well below the threshold value at which dynamic effects begin to play an important role, cf., [38]. Figure 7 depicts some measured hysteresis loops for the considered grade.

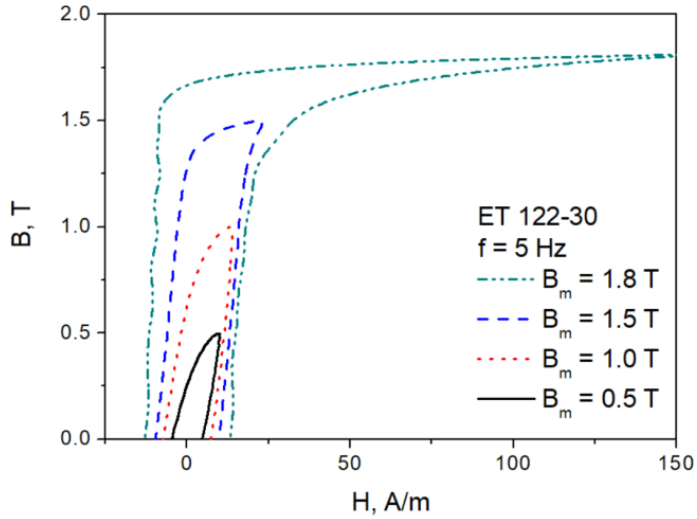

Figure 7. A family of measured hysteresis loops for ET 122-30 GO electrical steel.

In our computations we assumed that the major loop was obtained for $B_{\mathrm{m}} \cong 1.8$ T. For the major loop $b\left(H_{\mathrm{eff}}^{\mathrm{TIP}}, M^{\mathrm{TIP}}\right) \to 0$, the effect of varying slope of anhysteretic curves and hysteresis loop branches for different maximum flux densities (cf., Figure 6 for simulated curves in dimensionless units) was captured in the description by the update of $b\left(H_{\mathrm{eff}}^{\mathrm{TIP}}, M^{\mathrm{TIP}}\right)$ values for minor loops.

The estimation procedure is a bit awkward because magnetization appeared on both sides of (12) (it is included implicitly in the effective field). Thus, a nonlinear equation had to be solved for magnetization using, e.g., the Newton–Raphson method at each reference data point. The fitness indicator was the sum of squared deviations between the measured and the modeled magnetization values corresponding to the same preset field strength values. For estimation purposes we used the Matlab implementation of the robust DIRECT algorithm [39], developed by Finkel [40]. This code has been used previously and was found to be quite useful in solving the estimation problem for the Jiles–Atherton model [41]. The idea of the algorithm may be summarized as follows:

- Transformation of the n-dimensional search space into an n-dimensional hypercube with unit dimensions;
- Subdivision of the hypercube into smaller units and sampling of the fitness value (sum of squared deviations between the measured and modeled magnetization values corresponding to the same preset field strength values);
- Choice of the "most promising" unit for further processing;
- "Zoom" of the chosen unit into the n-dimensional hypercube and its successive processing according to the rule described above.

The modeling results for the major loop are depicted in Figure 8. The values of all parameters are also shown in the figure. It can be remarked that the estimated value of the "effective field" coefficient α was roughly equal to $H_{\mathrm{c}}/M_{\mathrm{s}}$ [41,42].

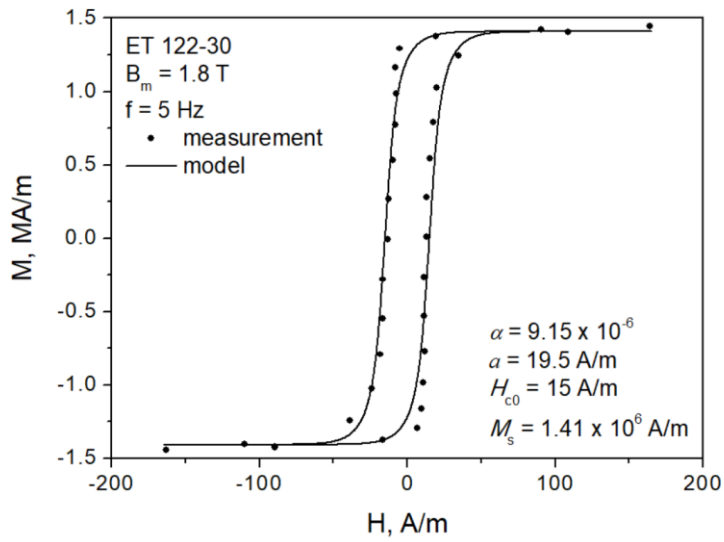

Figure 8. The measured and the modeled major loop for the considered grade.

In order to describe minor loops, it is clear that the substitutions $y = M/M_s$, $a_0 = H_c/a$ and $x = H_{eff}/a$ should hold. Two modeling strategies may be considered at this point:

- Model 1:

For a given amplitude of minor loop M_m, compute the equivalent amplitude y_m. Compute the reduced coercive field $a_0 = H_c/a$.

Next, following the algorithm outlined in the previous section, compute the hysteresis loop branches in the reduced units $x = \text{atanh}(y \mp b) \pm a_0$. Figure 9 depicts the simulated $x = x(y)$ (i.e., $h_{eff} = h_{eff}(m)$) hysteresis loops corresponding to $\mu_0 M_m = 0.5$ and 1 T.

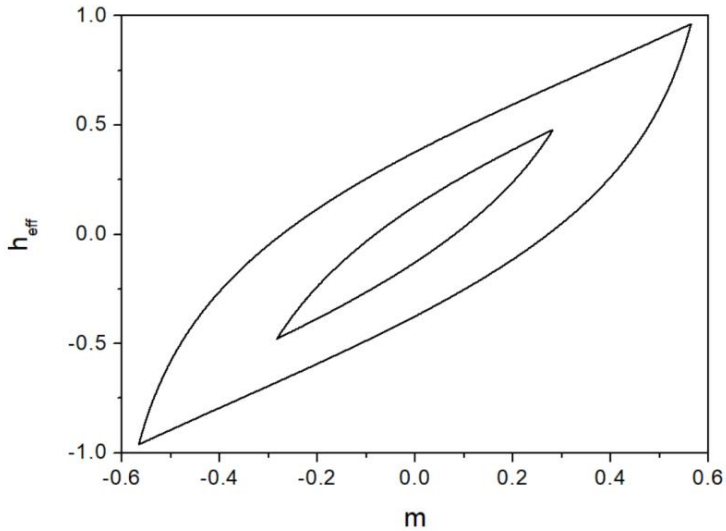

Figure 9. Simulated $h_{eff} = h_{eff}(m)$ loops corresponding to $\mu_0 M_m = 0.5$ and 1 T.

Substituting back $M = yM_s$ and $H = ax - \alpha M$, we obtain the sought hysteresis minor loop in physical units.

- Model 2:

This approach is based on geometric interpretation of the effective field related to the concept of affine transformation. A similar problem is defined in digital image processing as homography. The coordinates of any point P in the ordinary coordinates $(H,\ M)$ (thus also the major loop tip, used in subsequent computations) may be represented in the slanted coordinates $H_{eff} = H_{eff}(M)$ where the tangent of angle ϕ is equal to $\alpha M/H$, cf., Figure 10.

The relationship for the forward transformation may be derived by recalling the formula for rotation matrix in 2D by angle θ, which is

$$\begin{bmatrix} x_{\text{new}} \\ y_{\text{new}} \end{bmatrix} = \begin{bmatrix} \cos\theta & -\sin\theta \\ \sin\theta & \cos\theta \end{bmatrix} \begin{bmatrix} x_{\text{old}} \\ y_{\text{old}} \end{bmatrix} \tag{11}$$

However, in our case we just rotated the "dependent" (field-related) axis, thus

$$\begin{bmatrix} m \\ h_{\text{eff}} \end{bmatrix} = \begin{bmatrix} 1 & 0 \\ \sin\phi & \cos\phi \end{bmatrix} \begin{bmatrix} m \\ h \end{bmatrix} \tag{12}$$

where the symbols m, h, h_{eff} denote magnetization, field strength, and effective field strength in reduced units, respectively, and $\phi = -\text{atan}\left(\alpha M^{\text{TIP}} / H^{\text{TIP}}\right)$.

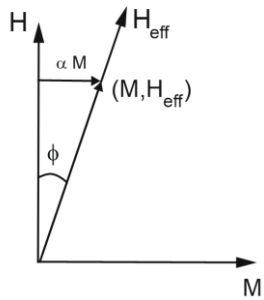

Figure 10. The coordinate systems $H = H(M)$ and $H_{\text{eff}} = H_{\text{eff}}(M)$.

The inverse transformation is given as

$$\begin{bmatrix} m \\ h \end{bmatrix} = \begin{bmatrix} 1 & 0 \\ -\tan\phi & 1/\cos\phi \end{bmatrix} \begin{bmatrix} m \\ h_{\text{eff}} \end{bmatrix} \tag{13}$$

Exemplary modeled minor loops are depicted in Figures 11 and 12. The value of coercive field strength in dimensionless units was taken from the parameters for the major loop, i.e., $a_0 = 15/19.5 \cong 0.769$. In Figure 11 the modeling results are shown for both models. It can be stated that model 1 described the experimental data slightly better than model 2 for the medium excitation amplitude; however, the shape of the minor hysteresis loop for the lower excitation amplitude was better reproduced with model 2. Modeled differential susceptibilities for model 2 were lower than for model 1 in both cases.

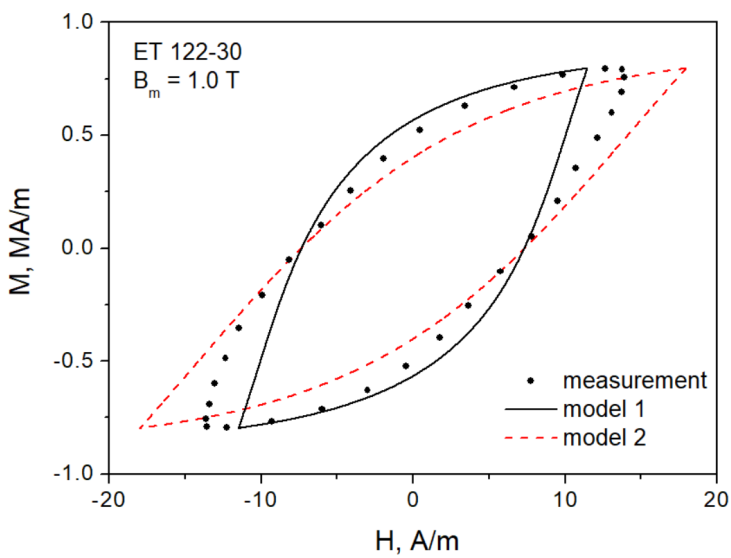

Figure 11. The measured and the modeled minor loop for $\mu_0 M_{\text{m}} \cong 1.0$ T.

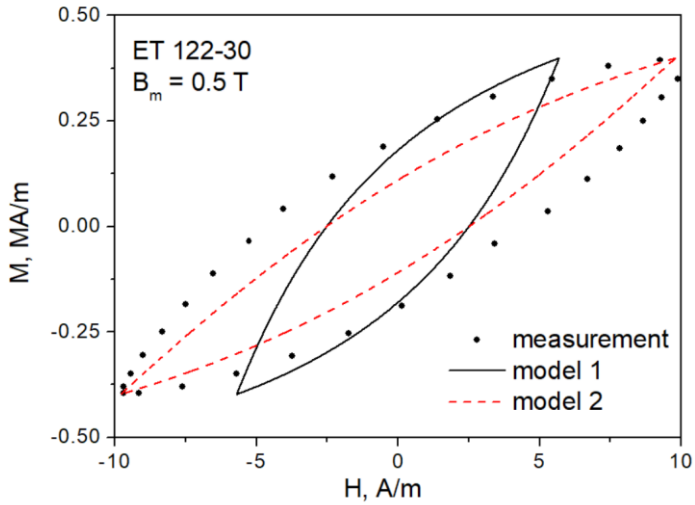

Figure 12. The measured and the modeled minor loop for $\mu_0 M_{\mathrm{m}} \cong 0.5$ T.

3.2. Extension to the Dynamic Conditions

An extension to the dynamic conditions may be carried out using the formalism presented in ref. [37]. The approach relies on the application of the power–law relationship considered by Zirka and coworkers [43] (who used it for the description of the excess field only) in order to describe the distortion of the loop shape due to eddy currents in different time–spatial scales generated in the conductive material. The proposed algorithm may be perceived as a special case of the Chua–Bass model [44]. A somewhat similar approach was considered in ref. [45].

The starting point for considerations is the dependence coercive field strength vs. frequency for the major loop. The results of measurements and their fitting to the fractional-type relationship $H_{\mathrm{c}} = H_{\mathrm{c0}} + Af^{\beta}$ are depicted in Figure 13.

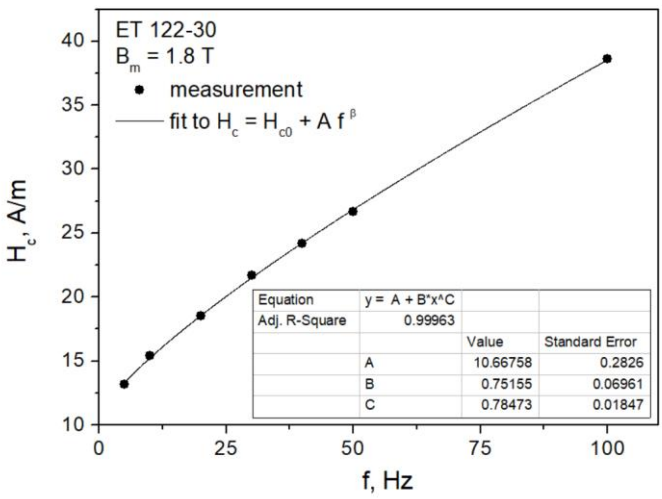

Figure 13. The measured and the modeled dependence $H_{\mathrm{c}} = H_{\mathrm{c}}(f)$.

The estimated value of exponent in the above-given relationship is used in successive computations. The fractional power law for determination of dynamic hysteresis loops is written as

$$H(t) = H_{\mathrm{stat}}(M) + \left[\frac{1}{K\left(1 - (M/M_s)^2\right)} \frac{dM}{dt} \right]^{\beta} \tag{14}$$

where the only fitting parameter is the normalization constant K appearing in the denominator of the second term of the expression.

Exemplary results of modeling minor loops under the increased excitation frequency are depicted in Figure 14. We chose the main frequency in Europe (50 Hz) since the results are of practical importance. It can be stated that the trends observed for quasi-static loops remained valid, i.e., modeled dynamic susceptibilities from model 2 were lower than for model 1. In order to perform a quantitative assessment of both models, we computed the discrepancies between measured and modeled coercivities and remanence magnetizations.

Model 1 underestimated the coercive field strength by 7.9%, whereas model 2 by 2.9%.

Model 1 overestimated the remanence magnetization by 7.7%, whereas model 2 underestimated this value by 7.8%. Therefore, it may seem that model 2 performed a little better. This observation may be confirmed by yet another figure of merit, namely, loop area, which corresponds to the dissipated energy loss. For model 1 the computed loss area was measured as smaller than its counterpart by 5.7%, whereas for model 2 by merely 0.2%.

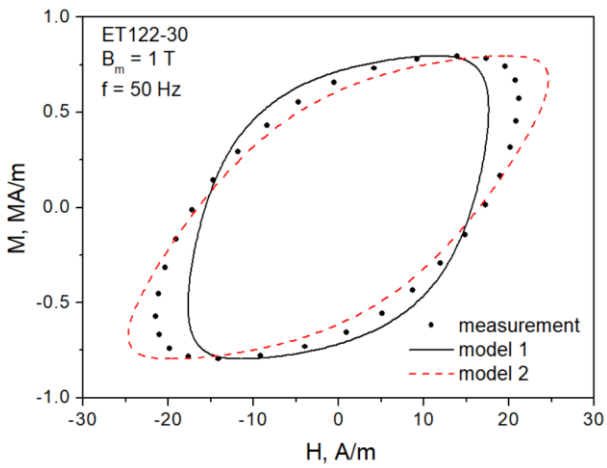

Figure 14. The measured and the modeled minor loops at $f = 50$ Hz.

4. Discussion

In the paper we verified the possibility to model minor hysteresis loops of grain-oriented steel with the phenomenological T(x) model in which one of the variables was identified as the "effective" field. We considered two possible approaches to carry out transformation from the "effective" field (which is not directly measurable) to the "ordinary" H field. It can be stated that both approaches might be useful.

It should be remembered that the considered approach takes into account the irreversible field component only. It is felt that further model refinement might be obtained by the introduction of additional functional dependences accounting for reversibility. Some preliminary results were presented previously in refs. [46,47].

A recent contribution [48] which considered a more general transformation based on hypergeometric functions also offered an improved description of minor loops in GO steel. However, to the best of our knowledge, a simple relationship similar to the hyperbolic tangent of a sum/difference of its arguments does not exist for hypergeometric functions. Such an expression would be needed for an explicit definition of the anhysteretic curve. Moreover, the advantage of the present approach is that it offers a tangible interpretation of anhysteretic curves and puts in the spotlight its deep connection to the hysteresis loop. It should be remembered that the considered models correspond to the conditions in which magnetic materials are characterized [49].

In order to let the readers obtain a more comprehensive picture of the advantages of the approach presented in this paper, we include here a brief discussion of some chosen papers concerning two other hysteresis models most commonly used in electrical engineering, namely the Preisach formalism [50,51] and the JA model.

The Preisach model is a phenomenological bottom–up approach in which the outcome hysteresis is the result of summing individual contributions from elementary units, referred to as hysterons. The model usually uses magnetic field strength as its input and magnetization as its output; thus, in order to adapt it to the conditions in which magnetic properties of materials are characterized [49], it is necessary to carry out additional numerical computations [52,53]. The fundamental issue for this description is the proper identification of the so-called hysteron density function.

Rouve et al. [54] compared several formulations for the hysteron density function and modeled hysteresis curves for a 0.27 mm thick GO steel sample. The relative errors for loop area (representing energy loss) in most cases were of the order 20%–40%. It is interesting to remark that the most promising implementation of the Preisach model takes into account the interaction term, which is equivalent to the use of the "effective field" such as in the present contribution.

Eichler et al. suggested that the use of a nonuniform grid applied to hysteron distribution might improve the overall performance of the Preisach model and its accuracy for hysteresis loops in GO steel [55]. The proposed approach allowed them to increase the computation speed by two orders of magnitude; however, it required more complicated pre-processing grid data necessary for modeling.

Naghizadeh et al. [56] focused on the identification issue for the JA model. The authors compared several metaheuristic methods (simulated annealing, genetic algorithms, differential evolution, particle swarm optimization and shuffled frog leaping algorithm) in terms of their ability to recover optimal values of JA model parameters for chosen grades of grain-oriented and non-oriented steel. Despite the authors being able to obtain quite-accurate representations of minor loops, it is remarkable that the parameter sets obtained with different methods were quite different. Moreover, it can be noticed that their values varied significantly upon changing the excitation amplitude; however, it is difficult to draw general meaningful conclusions about the observed trends. A similar problem may be noticed when analyzing the results of a recently published paper [57]. It is obvious that freeing the values of model parameters should in general yield better results than keeping them fixed or varying in accordance to some prescribed functional dependencies [58]; however, a question arises about the physical interpretation of parameter values and the validity of the proposed methodology.

The problem of estimating JA model parameters with meaningful physical interpretation has recently been addressed in refs. [59,60]. In these publications the authors proposed introducing some constraints between the values of some parameters which affect the shape of the "anhysteretic" curve in the JA model in order to be rid of some non-physical solutions, reported previously, e.g., in ref. [19]. It should be emphasized that in the considered T(x) model such problems do not exist.

As far as the dynamic extension of the hysteresis model is concerned, we would like to point the attention of the readers to some recent papers from the Durham team [61,62]. The authors were clearly inspired by Zirka's approach [43]; thus, they focused on the three-term separation formula in which a relationship similar to (14) was used for the description of "excess" field. As pointed out previously, our approach assumed that such an expression describes all dynamic contributions due to eddy currents in multiple time–spatial scales. It is remarkable that most probably due to the presence of a "classical" field term, Hamzehbahmani was forced to use different functional dependencies for the reciprocal of K in the formula equivalent to (14).

Future research may be focused on the following aspects:

1. An extended T(x) model may be used to describe hysteresis curves of a material subject to applied stress. It is expected that Sablik's extension to the effective field may be useful for this purpose [63];
2. The possibility to describe hysteresis curves in a ferromagnetic lamination when a T(x) model is applied on a local (microscopic, not bulk) scale and the coupling of the model with the finite element method using the solver implemented in the Argos suite should be explored [64,65].

3. The model should be extended to the case of biased and multi-harmonic excitation [66–68] and further validation of the description of dynamic properties should be performed.

5. Conclusions

In the present paper we showed the possibility to describe symmetric minor loops of grain-oriented steel with the phenomenological T(x) model, in which the variable x was interpreted as a reduced "effective" field. We have elucidated the deep relationship between anhysteretic curve and its hysteretic counterpart, i.e., the minor hysteresis loop. It can be stated that the T(x) framework provides a self-consistent description of both phenomena. We proved that, in fact, there exist families of anhysteretic curves. Two approaches for modeling the "effective" field have been considered. We showed that the combination of the T(x) model plus an additional dynamic term derived from the $H_c = H_c(f)$ dependence allows one to reproduce minor loops quite accurately. The presented results may hopefully be interesting to engineers working on hysteresis modeling and to physicists alike.

Author Contributions: Conceptualization, K.R.C., P.J., D.K., T.S., V.K. and P.K.; methodology, K.R.C.; software, P.J., D.K. and T.S.; validation, V.K. and P.K.; formal analysis, V.K. and P.K.; investigation, K.R.C., P.J., D.K. and T.S.; resources, K.R.C.; data curation, P.J., D.K. and T.S.; writing—original draft preparation, K.R.C.; writing—review and editing, P.J., D.K., T.S., V.K. and P.K.; visualization, K.R.C.; supervision, P.J.; project administration, P.J.; funding acquisition, K.R.C. All authors have read and agreed to the published version of the manuscript.

Funding: The authors are grateful to the Dean of Faculty of Electrical Engineering Marek Lis for partial financial support to cover the APC from statutory funds for research carried out at Faculty of Electrical Engineering, CUT, BS/PB-3-300-301/11/20/P.

Institutional Review Board Statement: Not applicable.

Informed Consent Statement: Not applicable.

Data Availability Statement: Data available from the corresponding author upon request.

Acknowledgments: The work of Polish authors was supported from a project within the framework of the Program No. 020/RID/2018/19 "Regional Initiative of Excellence" granted by the Minister of Science and High Education in the years 2019–2023, the amount of funding 12,000,000 PLN. From the project funds the costs of internship of these authors at University of West Bohemia in 2022 were covered.

Conflicts of Interest: The authors declare no conflict of interest.

Nomenclature

CGO	abbreviation for "Conventional Grain Oriented"(electrical steel)
HGO	abbreviation for "High Grain Oriented"
GO	abbreviation for "grain oriented"
JA	abbreviation for "Jiles-Atherton" (model)
a_0	dimensionless quantity in the T(x) model, interpreted as coercive field strength in reduced units
b	dimensionless quantity in the T(x) model, used to match loop tips so that they belong to the anhysteretic curve
x	dimensionless quantity in the T(x) model, interpreted as strength of applied field or effective field in reduced units
y	dimensionless quantity in the T(x) model, interpreted as magnetization in reduced units
T	abbreviated notation for hyperbolic tangent
α	mean field (Weiss') coefficient, accounting for mutual interactions between magnetic moments within ferromagnetic material, dimensionless
β	fractional coefficient which describes the evolution of coercive field strength upon excitation frequency increase (experimental data fitted with a power law plus free term)
a	shape parameter in the JA and the T(x) models, A/m, in the latter description it is used to adjust the value of the fraction subject to hyperbolic tangent transformation, cf. Equation (9)
H_c	coercive field strength for the major loop, A/m; subscript "0" in the section devoted to dynamic extension is meant to draw attention of the readers that this quantity refers to quasi-static limit
H_{eff}	effective field, A/m, in the simplest form defined as $H_{\mathrm{eff}} = H + \alpha M$
M_{s}	saturation magnetization, A/m

References

1. *C57.12.80-2010*; IEEE Standard Terminology for Power and Distribution Transformers. IEEE: Piscataway, NJ, USA, 2010. [CrossRef]
2. Amoiralis, E.I.; Tsili, M.; Kladas, A.G. Transformer design and optimization: A literature survey. *IEEE Trans. Power Deliv.* **2009**, *24*, 1999–2024. [CrossRef]
3. Sai Ram, B.; Paul, A.K.; Kulkarni, S.V. Soft magnetic materials and their applications in transformers. *J. Magn. Magn. Mater.* **2021**, *537*, 168210. [CrossRef]
4. Raabe, D. Electrical Steels—Iron-Silicon Transformer Steels. Available online: https://www.dierk-raabe.com/electrical-steels-fe-3-si/ (accessed on 2 February 2023).
5. Fiorillo, F.; Bertotti, G.; Appino, C.; Pasquale, M. Soft magnetic materials. In *The Wiley Encyclopedia of Electrical Engineering*; Webster, J.G., Ed.; Nova Science Publishers: New York, NY, USA, 2016. [CrossRef]
6. Rauscher, P.; Hauptmann, J.; Beyer, E. Laser scribing of grain oriented electrical steel under the aspect of industrial utilization using high power laser beam sources. *Phys. Proc.* **2013**, *41*, 312–318. [CrossRef]
7. Li, Y.; Song, S.; Dou, Y.; Chen, T. Influence of tensile stress on the magnetic properties of ultra-thin grain-oriented electrical steel. *AIP Adv.* **2023**, *13*, 025223. [CrossRef]
8. Takada, Y.; Abe, M.; Masuda, S.; Inagaki, J. Commercial scale production of Fe-6.5 wt. % Si sheet and its magnetic properties. *J. Appl. Phys.* **1988**, *64*, 5367–5369. [CrossRef]
9. Chwastek, K. Electrical Steel with Increased Silicon Content. In *Advances in Materials Research*; Wythers, M.C., Ed.; Nova Science Publishers: New York, NY, USA, 2019; Volume 36, pp. 207–217. Available online: https://novapublishers.com/shop/advances-in-materials-science-research-volume-36/ (accessed on 1 November 2022).
10. Moses, A.J. Energy efficient electrical steels: Magnetic performance prediction and optimization (Viewpoint paper). *Scr. Mater.* **2012**, *67*, 560–565. [CrossRef]
11. Kefalas, T.D.; Kladas, A. Harmonic Impact on Distribution Transformer No-Load Loss. *IEEE Trans. Ind. Electron.* **2010**, *57*, 193–200. [CrossRef]
12. Rauscher, P.; Betz, B.; Hauptmann, J.; Wetzig, A.; Beyer, E.; Grünzweig, C. The influence of laser scribing on magnetic domain formation in grain oriented electrical steel visualized by directional neutron dark-field imaging. *Sci. Rep.* **2016**, *6*, 38307. [CrossRef] [PubMed]
13. Korzunin, G.S. The modern status of inspection of certain magnetic characteristics of anisotropic electrical steel. *Rus. J. Nondestr. Test.* **2005**, *41*, 640–665. [CrossRef]
14. Davies, H.A.; Fiorillo, F.; Flohrer, S.; Guenther, H.; Hasegawa, R.; Sievert, J.; Varga, L.K.; Yamaguchi, M. Challenges in optimizing the magnetic properties of bulk soft magnetic materials. *J. Magn. Magn. Mater.* **2008**, *320*, 2411–2422.
15. Schneider, C.S.; Winchell, S.D. Hysteresis in conducting ferromagnets. *Phys. B Condens. Matter* **2006**, *372*, 269–272. [CrossRef]
16. Jiles, D.C.; Atherton, D.L. Theory of Ferromagnetic Hysteresis. *J. Magn. Magn. Mater.* **1986**, *61*, 48–60. [CrossRef]
17. Chwastek, K.; Szczygłowski, J. Estimation methods for the Jiles-Atherton model parameters–A review. *Przegl. Elektrotechn.* **2008**, *12*, 145–148.
18. Rupnik, U.; Alić, A.; Miljavec, D. Harmonization and validation of Jiles-Atherton static hysteresis models. *Energies* **2022**, *15*, 6760. [CrossRef]
19. Zirka, S.E.; Moroz, Y.I.; Harrison, R.G.; Chwastek, K. On Physical Aspects of the Jiles-Atherton Hysteresis Models. *J. Appl. Phys.* **2012**, *112*, 043916. [CrossRef]
20. Harrison, R.G. A Physical Model of Spin Ferromagnetism. *IEEE Trans. Magn.* **2003**, *39*, 950–960. [CrossRef]
21. Takács, J. *Mathematics of Hysteretic Phenomena*; Wiley-VCH: Weinheim, Germany, 2003.
22. Steinhaus, W.; Gumlich, E. Experimentelle Untersuchungen zur Theorie des Ferromagnetismus. II. Ideale, d.h. hysteresefreie Magnetisierung. (Experimental research on the theory of ferromagnetism. II. Ideal or hysteresis-free magnetization–in German). *Arch. Elektrotechnik* **1915**, *4*, 149–158. [CrossRef]
23. Mousavi, S.A.; Krings, A.; Engdahl, G.; Bissal, A. Measurement and Modeling of Anhysteretic Curves. In Proceedings of the 19th International Conference on the Computation of Electromagnetic Fields (COMPUMAG 2013), Budapest, Hungary, 30 June–4 July 2013. Available online: https://www.researchgate.net/publication/256692452_Measurement_and_Modeling_of_Anhysteretic_Curves (accessed on 2 February 2023).
24. Nowicki, M. Anhysteretic magnetization measurement methods for soft magnetic materials. *Materials* **2018**, *11*, 2021. [CrossRef]
25. Pearson, J.; Squire, P.T.; Atkinson, D. Which anhysteretic magnetization curve? *IEEE Trans. Magn.* **1997**, *33*, 3970–3972. [CrossRef]
26. Silveyra, J.M.; Conde Garrido, J.M. On the modelling of the anhysteretic magnetization of homogeneous soft magnetic materials. *J. Magn. Magn. Mater.* **2021**, *540*, 168430. [CrossRef]
27. Chwastek, K. Higher order reversal curves in some hysteresis models. *Arch. Electr. Eng.* **2012**, *61*, 455–470. [CrossRef]
28. Raghunathan, A.; Melikhov, Y.; Snyder, J.E.; Jiles, D.C. Modeling of Two-Phase Magnetic Materials Based on Jiles–Atherton Theory of Hysteresis. *J. Magn. Magn. Mater.* **2012**, *324*, 20–22. [CrossRef]
29. Takács, J.; Mészáros, I. Separation of magnetic phases in alloys. *Phys. B Condens. Matter* **2008**, *403*, 3137–3140. [CrossRef]
30. Baric, T.; Boras, V.; Glavas, H. Advantages of Dual Hyperbolic Tangent Function Over Single Hyperbolic Tangent Function in Description of Hysteresis Loops. *Int. Rev. Electr. Eng.* **2016**, *11*, 506–516.
31. Gozdur, R.; Gębara, P.; Chwastek, K. A Study of Temperature-Dependent Hysteresis Curves for a Magnetocaloric Composite Based on La(Fe, Mn, Si)13-H Type Alloys. *Energies* **2020**, *13*, 1491. [CrossRef]

32. Takács, J. Mathematical proof of the definition of anhysteretic state. *Phys. B Condens. Matter* **2006**, *372*, 57–60. [CrossRef]
33. Krah, J.H.; Bergqvist, A.J. Numerical Optimization of a Hysteresis Model. *Phys. B Condens. Matter* **2004**, *343*, 35–38. [CrossRef]
34. Chwastek, K. A dynamic extension to the Takács model. *Phys. B Condens. Matter* **2010**, *405*, 3800–3802. [CrossRef]
35. Atherton, D.L.; Ton, V. The effects of stress on a ferromagnet on a minor hysteresis loop. *IEEE Trans. Magn.* **1990**, *26*, 1153–1156. [CrossRef]
36. Sablik, M.J.; Langman, R.A. Approach to the anhysteretic surface. *J. Appl. Phys.* **1996**, *79*, 6134–6136. [CrossRef]
37. Chwastek, K. The effects of sheet thickness and excitation frequency on hysteresis loops of non-oriented electrical steel. *Sensors* **2022**, *22*, 7873. [CrossRef]
38. Haller, T.R.; Kramer, J.J. Observation of dynamic domain size variation in a silicon-iron alloy. *J. Appl. Phys.* **1970**, *41*, 1034–1035. [CrossRef]
39. Jones, D.R. The DIRECT global optimization algorithm. In *Encyclopedia of Optimization*; Kluwer Academic Publishers: Boston, MA, USA, 2001; Volume 1, pp. 431–440.
40. Finkel, D.E. Research and Codes. Available online: https://ctk.math.ncsu.edu/Finkel_Direct/ (accessed on 1 November 2022).
41. Chwastek, K.; Szczygłowski, J. An alternative method to estimate the parameters of Jiles-Atherton model. *J. Magn. Magn. Mater.* **2007**, *314*, 47–51. [CrossRef]
42. Basso, V.; Bertotti, G.; Infortuna, A.; Pasquale, M. Preisach Model Study of the Connection between Magnetic and Microstructural Properties of Soft Magnetic Materials. *IEEE Trans. Magn.* **1995**, *31*, 4000–4005. [CrossRef]
43. Zirka, S.E.; Moroz, Y.I.; Marketos, P.; Moses, A.J.; Jiles, D.C.; Matsuo, T. Generalization of the Classical Method for Calculating Dynamic Hysteresis Loops in Grain-Oriented Electrical Steels. *IEEE Trans. Magn.* **2008**, *44*, 2113–2125. [CrossRef]
44. Chua, L.; Bass, S.C. A Generalized Hysteresis Model. *Int. J. Eng. Sci.* **1971**, *19*, 36–45. [CrossRef]
45. De León, F.; Semlyen, A. A simple representation of dynamic hysteresis losses in power transformers. *IEEE Trans. Power Deliv.* **1995**, *10*, 315–320. [CrossRef]
46. Chwastek, K.; Baghel, A.P.S.; Sai Ram, B.; Borowik, B.; Daniel, L.; Kulkarni, S.V. On some approaches to model reversible magnetization processes. *J. Phys. D Appl. Phys.* **2018**, *51*, 145003. [CrossRef]
47. Jastrzębski, R.; Jakubas, A.; Chwastek, K. A comparison of two phenomenological descriptions of magnetization curves based on the T(x) model. *Acta Phys. Pol. A* **2019**, *136*, 720–723. [CrossRef]
48. Herceg, D.; Chwastek, K.; Herceg, Đ. The use of hypergeometric functions in hysteresis modeling. *Energies* **2020**, *13*, 6500. [CrossRef]
49. Fiorillo, F. *Measurement and Characterization of Magnetic Materials*; Academic Press: Amsterdam, The Netherlands, 2004.
50. Preisach, F. Über die magnetische Nachwirkung (On magnetic magnetoeffect–in German). *Z. Phys.* **1935**, *94*, 277–302. [CrossRef]
51. Mayergoyz, I.D. *Mathematical Models of Hysteresis and Their Applications*; Elsevier: New York, NY, USA, 2003.
52. Bernard, Y.; Mendes, E.; Santandrea, L.; Bouillault, F. Inverse Preisach model in finite elements modelling. *Eur. Phys. J.* **2000**, *12*, 117–121. [CrossRef]
53. Bi, S.; Wolf, F.; Lerch, R.; Sutor, A. An inverted Preisach model with analytical weight function and its numerical discrete formulation. *IEEE Trans. Magn.* **2014**, *50*, 7300904. [CrossRef]
54. Rouve, L.-L.; Waeckerlé, T.; Kedouc-Lebouc, A. Application of Preisach Model to Grain Oriented Steels: Comparison of Different Characterizations for the Preisach Function p(α, β). *IEEE Trans. Magn.* **1995**, *31*, 3557–3559. [CrossRef]
55. Eichler, J.; Novak, M.; Kosek, M. Experimental Determination of the Preisach Model for Grain Oriented Steel. *Acta Phys. Pol. A* **2018**, *136*, 713–719. [CrossRef]
56. Naghizadeh, R.-A.; Vahidi, B.; Hosseinian, S.H. Parameter identification of Jiles-Atherton model using SFLA. *Compel* **2012**, *31*, 1293–1309. [CrossRef]
57. Chen, L.; Wen, X.; Ben, T.; Jing, L.; Liu, Q. Accurate calculation of global hysteresis properties of grain-oriented silicon steel based on an improved J-A model with variable parameters. *AIP Adv.* **2023**, *13*, 025254. [CrossRef]
58. Chwastek, K.; Szczygłowski, J.; Wilczyński, W. Modeling dynamic hysteresis loops in steel sheets. *Compel* **2009**, *28*, 603–612. [CrossRef]
59. Padilha, J.B.; Kuo-Peng, P.; Sadowski, N.; Leite, J.V.; Batistela, N.J. Restriction in the determination of the Jiles-Atherton hysteresis model parameters. *J. Magn. Magn. Mater.* **2017**, *442*, 8–14. [CrossRef]
60. Upadhaya, B.; Rasilo, P.; Perkkiö, L.; Handgruber, P.; Belahcen, A.; Arkkio, A. A constraint-based optimization technique for estimating physical parameters of Jiles-Atherton hysteresis model. *Compel* **2020**, *39*, 1281–1298. [CrossRef]
61. Hamzehbahmani, H. Static hysteresis modeling for grain-oriented electrical steels based on the phenomenologic concepts of energy loss mechanism. *J. Appl. Phys.* **2021**, *130*, 055102. [CrossRef]
62. Zhang, Z.; Hamzehbahmani, H.; Gaskell, P.H. A Novel Dynamic Hysteresis Model for Grain-Oriented Electrical Steels Based on Magnetic Domain Theory. *IEEE Trans. Magn.* **2022**, *58*, 7300109. [CrossRef]
63. Sablik, M.J.; Jiles, D.C. A model for hysteresis in magnetostriction. *J. Appl. Phys.* **1988**, *64*, 5402–5404. [CrossRef]
64. Orosz, T.; Pánek, D.; Karban, P. FEM Based Preliminary Design Optimization in Case of Large Power Transformers. *Appl. Sci.* **2020**, *10*, 1361. [CrossRef]
65. Karban, P.; Pánek, D.; Orosz, T.; Petrášova, I.; Doležel, I. FEM based robust design optimization with Agros and Ārtap. *Comput. Math. Appl.* **2021**, *81*, 618–633. [CrossRef]

66. Zhao, X.; Wang, R.; Liu, X.; Li, L. A Dynamic Hysteresis Model for Loss Estimation of GO Silicon Steel under DC-Biased Magnetization. *IEEE Trans. Ind. Appl.* **2020**, *57*, 409–416. [CrossRef]
67. Zhao, Z.; Hu, X.; Bi, Z.; Xu, M.; Ma, X.; Zhang, P. Calculation of core loss under distorted flux density with minor hysteresis loops for laminated steel structure. *AIP Adv.* **2020**, *10*, 075001. [CrossRef]
68. Zhao, H.; Liu, W.; Zhao, X.; Wu, Y. Magnetic loss in grain-oriented Fe–Si sheets under different harmonic excitation and high indication. *AIP Adv.* **2023**, *13*, 015208. [CrossRef]